Stochastic Voronoi Tessellations as Models for Cellular Neighborhoods in Simple Multicellular Organisms

Anand Srinivasan,* Steph S.M.H. Höhn,† and Raymond E. Goldstein‡
Department of Applied Mathematics and Theoretical Physics, Centre for Mathematical Sciences, University of Cambridge, Wilberforce Road, Cambridge CB3 0WA, United Kingdom
(Dated: March 11, 2024)

Recent work on distinct multicellular organisms has revealed a hitherto unknown type of biological noise; rather than a regular arrangement, cellular neighborhood volumes, obtained by Voronoi tessellations of the cell locations, are broadly distributed and consistent with gamma distributions. We propose an explanation for those observations in the case of the alga *Volvox*, whose somatic cells are embedded in an extracellular matrix (ECM) they export. Both a solvable one-dimensional model of ECM growth derived from bursty transcriptional activity and a two-dimensional "Voronoi liquid" model are shown to provide one-parameter families that smoothly interpolate between the empirically-observed near-maximum-entropy gamma distributions and the crystalline limit of Gaussian distributions governed by the central limit theorem. These results highlight a universal consequence of intrinsic biological noise on the architecture of certain tissues.

Some of the simplest multicellular organisms consist of tens, hundreds, or thousands of cells arranged in an extracellular matrix (ECM), a network of proteins and biopolymers secreted by the cells. They often have a simple geometry: linear chains and rosettes of choanoflagellates [1, 2], sheets and spheres of algae [3], and cylinders of sponges [4]. While at first glance the arrangement of cells in the ECM appears regular, recent work [5] revealed a hitherto undocumented disorder found by assigning neighborhoods to cells through a Voronoi tessellation based on cell centers. Strikingly, both the lab-evolved "snowflake yeast" [6] (a ramified form found after rounds of selection for sedimentation speed) and the alga *Volvox carteri* have broad distributions of Voronoi volumes v accurately fit by k-gamma distributions

$$p(v) = \frac{1}{\bar{v} - v_c} \frac{k^k x^{k-1}}{\Gamma(k)} \exp(-kx), \quad x = \frac{v - v_c}{\bar{v} - v_c}, \qquad (1)$$

where $\bar{v}$ is the mean volume and v_c is the cell size. Particularly for *Volvox*, these observations are central to a general question in developmental biology: *How do cells produce structures external to themselves in an accurate and robust manner?*

Volvox is one of the simplest multicellular systems with which to study statistical fluctuations in ECM generation. The adult (Fig. 1(a)) consists of $\sim 10^3$ somatic cells embedded at the surface of a transparent ECM, the uppermost layer of which is a thin elastic shell $\sim 500\,\mu$m in diameter and $\sim 30\,\mu$m thick, with a more gelatinous interior below; the organism is $> 98\%$ ECM. Daughter colonies develop from germ cells below the outer layer through rounds of binary division that yield a raft of cells held together by cytoplasmic bridges remaining after incomplete cytokinesis. Following "embryonic inversion" that turns the raft inside-out [7], daughters enlarge by export of ECM proteins, expanding the colony to its final size over the course of a day, during which the widely-distributed neighborhood volumes appear. Figure 1(a) shows a a section of the Voronoi tessellation obtained by light-sheet imaging [5]. The area distribution of Voronoi partitions across 6 organisms is shown in Fig. 1(b) along with a fit of the gamma distribution (1) that yields $k \approx 2.35 \pm 0.04$ (95% CI).

The general issue above becomes the question of how cells generate ECM so that the spheroidal form is maintained during the dramatic colony growth despite the strong right-skew of the neighborhood volume distribution (1). A biological answer might invoke cell signaling in response to mechanical forces as a mechanism to coordinate growth and would ascribe the distribution (1) to imperfections in that process. Surprisingly, the novel problem of neighborhood distributions is so little-studied that we do not even understand quantitatively the feedback-free case, surely a benchmark for any analysis of correlations. Work in granular physics [8] has shown that (1) arises from maximizing entropy of partitions subdividing a volume subject to a fixed mean partition size. But this begs the question of why biological systems should follow a maximum-entropy principle.

Here we study perhaps the simplest models for cellular positioning within a thin ECM, where noisy matrix production by statistically identical cells causes them to space apart randomly during growth. We formulate the resulting stochastic cellular configuration as a *point process* [9] whose Voronoi tessellation is a well-studied topic in stochastic geometry [10] and serves as a model for cellular neighborhoods. A class of analytically solvable 1D models is used to illustrate how gamma distributions (1) may arise from feedback-free growth processes, and a one-parameter family of 2D stochastic Voronoi tessellations is introduced as a prototype of systems with interactions between polygons. The following is a non-technical summary; details are in Supplementary Material [11]. In the following, capital letters $X_{i;\theta_1,\ldots}$ denote random variables (r.v.s) i with parameters $\theta_1, \ldots$, and W, X, Y, Z denote Gaussian, exponential, gamma, and beta r.v.s.

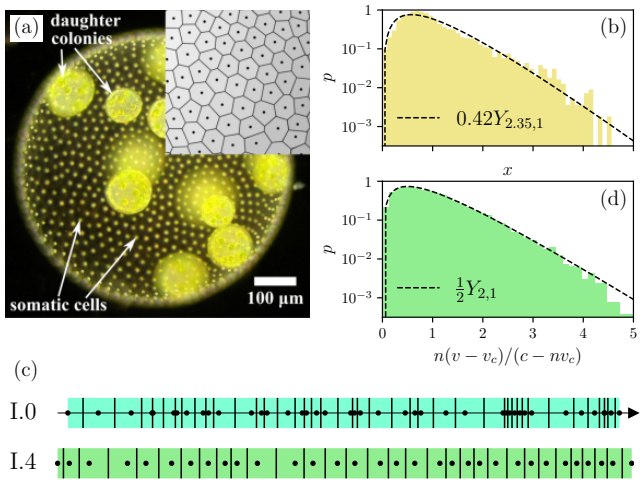

FIG. 1: The green alga *Volvox* and 1D models for cell positions. (a) Adult with cell types labelled, and section of Voronoi tessellation around somatic cells (dots within each Voronoi polygon), adapted from [5]. (b) Voronoi areas x follow the translated gamma distribution (1), computed by a fit of k. (c) Model I.1 [11], the Poisson process on $[0,\infty)$, where cells are indicated by dots, Voronoi boundaries by vertical line segments and intercalating ECM is colored. Model I.4, the circular Poisson process with minimum spacing. (d) Numerical distribution for model I.4, with no cell overlaps, compared to the analytical gamma distribution for large n.

In an act of extreme reductionism, consider a linear *Volvox* (termed model I.0 [11]). The gamma distribution has the property of being self-*divisible*, that is, $Y_{1;k,\lambda} = Y_{2;\frac{k}{2},\lambda} + Y_{3;\frac{k}{2},\lambda}$ for independent Y_2, Y_3 by the convolution rule for sums of random variables [11]. In a 1D ECM (Fig. 1c), if L_i are the cellular spacings then $V_i = (L_i + L_{i+1})/2$ are its Voronoi segments, which suggests the decomposition of V_i into spacings L_i which are themselves independent and identically distributed (i.i.d.) gamma r.v.s. Similarly, L_i is itself interpretable as arising from i.i.d. gamma-distributed mass increments during growth. This leads to two classes (i, ii) of configurations which one may expect to observe experimentally. The first (i) is that where L_i is formed by a large number k of small random mass increments, where k-gamma converges to a Gaussian by the central limit theorem, and at fixed mean to a delta distribution [11].

The second (ii) is the case in which L_i is formed by a small number of large mass increments, suggesting some intermediate piece comprising the ECM is produced at low copy number. A plausible precedent for fluctuations possessing this particular distribution is the bursting protein transcriptional activity observed in simple unicellular organisms such as *E. coli* [29]. There, it is known that mRNA transcription occurs at some rate when a gene is turned on, individual mRNA molecules are transcribed at some rate into proteins before degrading (e.g. by RNases) with an exponentially-distributed lifetime, and individual protein bursts exported into the extracellular environment correspond 1-1 with individual mRNA transcripts within the cell. Translating this phenomenology to *Volvox*, we hypothesize that $L_i \propto P_i$ where P_i is the steady-state extracellular concentration of a protein P governing ECM assembly. Then the time-dependent concentration $P_i(t)$ is a pure-jump process with some total number b of exponentially-distributed bursts, resulting in the b-gamma-distributed spacings $L_i = Y_{i;b,\lambda}$. (Fractional values of b, representing cross-cell averages, yield the same stationary b-gamma distribution, as shown from the master equation for $P_i(t)$ with exponential kernel [30]. We take $b \geq 1$ as every cellular neighborhood grows in *Volvox* without cell division.) Then, V_i is $2b$-gamma distributed,

$$V_i = \frac{X_{j;\lambda} + X_{j+1;\lambda}}{2} = \frac{1}{2} Y_{i;2b,\lambda} \overset{\text{pdf}}{\sim} \frac{4\lambda^{2b} v^{2b-1} e^{-2\lambda v}}{\Gamma(2b)}, \tag{2}$$

which, apart from the offset v_c, is (1) with $k = 2b$. That $k \approx 2.4$ in *Volvox*, approaching the 1D lower bound of $k = 2$ and apparently falling in class (ii), is consistent with observations that ISG, a glycoprotein critical to the ECM organization, is transcribed over a period of 10 minutes, quite short compared to its accumulation in the extracellular matrix over timescales comparable to the 48h life cycle [31].

In the low-copy number limit $b \to 1$, cellular positions $R_i = \sum_{j \leq i} L_j$ occur as a Poisson process. This is the maximum-entropy configuration, in which cell positions are uncorrelated in the sense that for any fixed number of cells N occurring within a fixed segment of size L, $\{R_i\}_{i=1}^N$ are i.i.d. uniform random variables [11]. Of course, the gamma distribution is supported on $[0,\infty)$ and one must consider finite-size effects. It can be shown [11] that on a circular ECM of fixed circumference C with fixed or variable cell count N (termed models I.1-I.3), the marginal distribution of Voronoi lengths given the above converges in the large-C, N limits at fixed cell number density to the same $2b$-gamma distribution—analogous to the convergence of ensembles in statistical physics in the thermodynamic limit.

To complete the 1D analysis, we show that the offset v_c in (1) from finite cell sizes. Suppose cells with centers of mass at $\{R_i\}_{i=1}^n$ on a circle of circumference c have uniform size v_c with $nv_c \leq c$, so that $L_i \geq v_c$ for all i. As we are in 1D, this is expressible as $L_i = v_c + \tilde{L}_i$, where $\tilde{L}_i$ are the random spacings of a smaller circle of circumference $c - nv_c$. This reduces to the fixed-N, C case of model I.2, hence we have the marginal Beta distribution for Voronoi lengths

$$V_i = v_c + \frac{c - nv_c}{2} Z_{i;2b,(n-2)b}. \tag{3}$$

Defining the cell number density within the remainder as $\rho = (n-2)/(c - nv_c)$ and taking the thermodynamic

limit $n, c \to \infty$ with ρ and v_c fixed, we have [11]

$$V_i = v_c + \frac{n-2}{2\rho} Z_{i;2b,(n-2)b} \overset{n\to\infty}{\longrightarrow} v_c + Y_{i;2b,2\rho}. \tag{4}$$

Thus, the lengths V_i with $2\rho := \lambda$ in (4) have precisely the distribution (1) under the substitution $\lambda = k/(\overline{v}-v_c)$.

Unlike in 1D where any sequence of partitions forms the real line, cells in 2D are nearly always interacting since their neighborhoods are mutually constrained to be a subdivision of the ECM. Their positions are derived from the neighborhood configurations, as ECM is secreted during growth, and we should expect that within a Voronoi description the cell locations will depend on those partitions. These geometric constraints co-exist with the possibility of maximum-entropy (Poisson) and minimum-entropy (crystalline) configurations. The family of point processes we introduce below models cellular interactions based on their Voronoi tessellations, interpolates between these phases, and can be interpreted as arising from a strain energy in each neighborhood. Our focus on geometry is complementary to recent work on topological properties of tessellations [32].

Let the ECM now be a bounded domain $\Omega \subset \mathbb{R}^2$, with area $|\Omega| > 0$ and a fixed number n of cells. We assume that cells are scattered at positions $\{\boldsymbol{x}_i\}_{i=1}^n = \mathcal{X}$ with cellular neighborhoods $\{D_i\}_{i=1}^n = \mathcal{D}$ comprising Ω in a manner which minimizes

$$E(\mathcal{X}, \mathcal{D}) = \frac{1}{2} \sum_{i=1}^{n} \int_{D_i} \|\boldsymbol{x} - \boldsymbol{x}_i\|^2 \, d\boldsymbol{x}, \tag{5}$$

Each summand of (5) is the trace of D_i's second area moment about $\boldsymbol{x}_i$, which for polygonal D_i is the small-strain limit of the bulk energy of a deformation from a regular n-gon centered at $\boldsymbol{x}_i$ [33]. Alternatively, minimizing E has the interpretation of an optimal cell-placement problem with a cost for transporting resources produced by cells at $\boldsymbol{x}_i$ to other points $\boldsymbol{x}$ in the neighborhoods D_i.

For fixed cell positions $\mathcal{X}$, the set $\mathcal{D}$ minimizing E is precisely the Voronoi tessellation of $\mathcal{X}$. To see this, note that for Voronoi $\mathcal{D}$, any other $\mathcal{D}'$, and a point $\boldsymbol{y}$ falling in $D_i \in \mathcal{D}$ and also in $D_i' \in \mathcal{D}'$, we have $\|\boldsymbol{y} - \boldsymbol{x}_i'\| \geq \|\boldsymbol{y} - \boldsymbol{x}_i\|$ by the Voronoi rule, hence $E(\mathcal{X}, \mathcal{D}') \geq E(\mathcal{X}, \mathcal{D})$. Rescaling the coordinates $\boldsymbol{x} \mapsto \boldsymbol{x}\sqrt{\rho}$ to achieve unit number density $\rho = n/|\Omega| \mapsto 1$, this motivates the study of the positional energy

$$V(\mathcal{X}) = \rho^2 E(\mathcal{X}, \mathrm{Vor}(\mathcal{X})), \tag{6}$$

where $\mathrm{Vor}(\mathcal{X})$ is the Voronoi tessellation. For fixed neighborhoods $\mathcal{D}$, calculating $\partial E/\partial \boldsymbol{x}_i = 0$ shows that the minimizing positions $\mathcal{X}$ are the $\mathcal{D}$-centroids $\boldsymbol{\mu}_i = |D_i|^{-1} \int_{D_i} \boldsymbol{x} d\boldsymbol{x}$; minimizers of V are *centroidal Voronoi tessellations* (CVTs), ubiquitous in meshing problems, clustering, and models of animal behavior [34].

Define a family of Gibbs point processes [10] whose joint positional distributions conditional on fixed N are

$$f_\beta(\mathcal{X}) \propto \exp\left(-\beta V(\mathcal{X})\right), \tag{7}$$

indexed by a temperature-like quantity β^{-1}. Following others who have investigated phase transitions of this system [35], we refer to it as the *Voronoi liquid*, which differs from classical pair-potential fluids due to many-body interactions between Voronoi-incident particles.

The maximum-entropy case (ii) is realized in the infinite-temperature limit $\beta \to 0$ with equiprobable configurations. This defines the "Poisson-Voronoi tessellation" (PVT) [10], which reduces to the exponentially-distributed spacings discussed in the 1D models above. The areas $|D_i|$ of 2D PVTs, a realization of which is shown in Fig. 2(d), have been shown in numerical studies to conform to k-gamma distributions [36–38]. A minimum-entropy configuration arises in the zero-temperature limit $\beta \to \infty$, where (7) becomes degenerate and the configuration freezes to a hexagonal lattice as in Fig. 2(d), which is the globally optimal CVT and densest sphere-packing in 2D [39]. Prior approaches using a structure factor analysis [40] found that, by contrast, Lloyd iterations (corresponding to a "fast quench" at zero temperature [41]) suppress crystalline configurations and adopt amorphous "hyperuniform" states. We investigate now the finite-temperature range $\beta \in (0, \infty)$, and show that areas are accurately described by k-gamma distributions with k an "order parameter" following a monotone relationship with β, analogous to the burst-count-driven spacing distributions of the 1D case.

As a generalization of our previous comment on nonuniqueness, in 2D the entropies of the Voronoi size distribution and of the positional distribution do not necessarily follow a monotone relation. *Volvox* itself (Fig. 1b) provides an example; its scaled area distribution (1) has $k \approx 2.3$, while Poisson-Voronoi tessellations of the flat torus and sphere have $k \approx 3.5$ [11], yet their positional distribution is the maximum-entropy one. Hence, "entropy" could refer to the differential entropy of its Voronoi size distribution *or* to that of its joint distribution over positions at fixed N.

Since V is C^2 [34], (7) is the stationary solution of a Langevin equation

$$dR_i(t) = -\left.\frac{\partial V}{\partial x_i}\right|_{\{R_j(t)\}} dt + \sqrt{2\beta^{-1}} dW_i(t), \tag{8}$$

with $W_i(t)$ i.i.d. Brownian motions, and time has been rescaled to $\beta^{-1}t$ to allow integration in the limit $\beta \to \infty$. Since $\partial V/\partial \boldsymbol{x}_i \propto |D_i|(\boldsymbol{x}_i - \boldsymbol{\mu}_i)$ [11], (8) may be interpreted as a neighborhood-centroid-seeking model of cellular dynamics during noisy growth or a Markov Chain Monte Carlo (MCMC) method to sample the stationary distribution (7). An Euler-Maruyama discretization of (8) does not satisfy detailed balance, but this can be

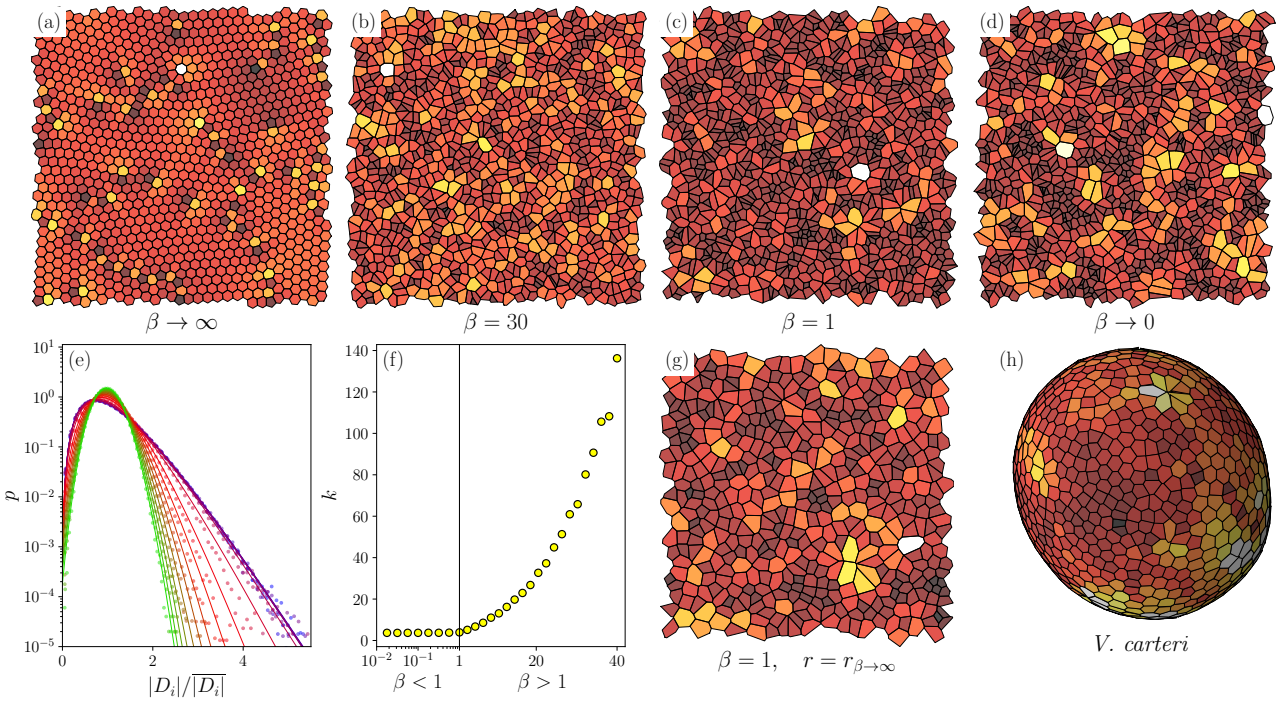

FIG. 2: Voronoi liquid interpolates between maximum- and minimum-entropy point configurations in 2D. (a)-(d): Monte Carlo simulations of the Voronoi liquid at varying temperatures, from the infinite-temperature (Poisson) limit to the zero-temperature (sphere-packing) limit. (e): Area distributions at all temperatures are approximately k-gamma distributed, with k monotone increasing with β. (f): k is constant for $\beta < 1$ and begins to grow superlinearly for $\beta > 1$. (g) Voronoi tessellation of *V. carteri* [11]. (h): Minimum spacing r enforced by the Matérn thinning rule [11], with r equal to the minimum spacing in the frozen limit $\beta \to \infty$. Voronoi polygons are colored from black to white based on relative area in each panel.

rectified by adding a Metropolis-Hastings step [11, 42]. Using this method, we investigated the statistical properties of the Voronoi liquid by numerically solving (8) for $n = 10^3$ [11], the somatic cell count of *Volvox*, in the simplified geometry of a unit square with periodic boundary conditions to remove curvature and topology effects.

Figures 2(a-d) show samples of the Voronoi liquid at varying temperatures with evident differences and similarities to *Volvox*. As seen in Fig. 2(e,f), area distributions sampled at 13 logarithmically spaced values from $\beta = 10^{-3} - 1$ and 21 linearly spaced values from $1 - 40$, are well-described by k-gamma distributions with k increasing monotonically with β. This is consistent with the transition of $p(|D_i| \,/\, \overline{|D_i|})$ to a parabola on the log-scale in Fig. 2e, the limit in which k-gamma approaches a Gaussian. It is in this sense that the control parameter β is analogous to the protein burst count b in 1D. A similar monotone relationship between the "granular temperature" β_{gr}^{-1} of a packing and k, in which partition size instead played the role of energy, has been noted previously in granular physics [8, 43].

The importance of intermediate-entropy configurations is perhaps more readily seen in 2D. Studies of confluent tissue [44] found that k-gamma distributions also arise in the aspect ratios (defined from the eigenvalues of the second area moment). Poisson-Voronoi tessellations, notably, do not possess gamma-distributed aspect ratios. They instead follow an approximate beta-prime distribution, perhaps as a consequence of the gamma-distributed principal stretches [11]. This is seen in Fig. 2(a), where high-aspect ratio "shards" occur at $\beta = 0$, yet disappear at low temperature. This raises questions of the underlying physics responsible for aspects of stochastic geometry than size. As a simple extension, the Voronoi liquid with hard-sphere thinning [11] (one way to produce the offset v_c (1) in 2D), a realization of which is shown in Fig. 2(h), does not exhibit these artifacts and more closely resembles the regular arrangement observed in *Volvox*, with both gamma-distributed areas and aspect ratios [11].

A biological interpretation of the Voronoi assumption is that the polygonal boundaries of each cellular neighborhood are the colliding fronts of isotropically produced ECM material exported from cells. Inverting the typical modelling procedure by *assuming* that the Voronoi rule holds at some temperature β^{-1}, one can infer the distributional parameters using standard maximum-likelihood estimators for Gibbs point processes [45]. From the estimated temperature, for example, one can invert the k-β relationship by monotonicity to deduce the copy number of bursty rate-limiting steps in growth. Such estima-

tors are critical for elastic models of tissues, where noise in individual cellular configurations co-exists with stable geometric properties of the population. The stochastic Voronoi models we have presented here reproduce aspects of configurational noise, such as the empirically observed gamma distributions, and simultaneously provide a formal framework—an ensemble—within which to infer features of random finite configurations of cells such as interaction strength and preferential geometry.

As a purely mathematical construct, a Voronoi tessellation makes no reference to microstructure around cells, and it thus plays a role for tissues analogous to the random walk model of polymers and the hard sphere model of fluids. Yet, each *Volvox* somatic cell sits within a polygonal "compartment" whose boundaries are composed of denser material within the larger ECM [46]. Dimly visible in brightfield microscopy, these compartments have recently been labelled fluorescently [47], enabling the simultaneous motion tracking of cells and growth of compartments during development. The strong correlation observed [47] between the location of these compartment boundaries and the the associated Voronoi partitions will enable tests of the connection hypothesized here between properties of stochastic ECM generation at the single cell level and population-level statistics.

We are grateful to T. Day, P. Yunker, and W. Ratcliff for numerous discussions. This work was supported in part by the Cambridge Trust (AS), The John Templeton Foundation and Wellcome Trust Investigator Grant 207510/Z/17/Z (SSMHH, REG).

* as3273@cam.ac.uk
† sh753@cam.ac.uk
‡ R.E.Goldstein@damtp.cam.ac.uk

[1] M.J. Dayel, R.A. Alegado, S.R. Fairclough, T.C. Levin, S.A. Nichols, K. McDonald, and N. King, Cell differentiation and morphogenesis in the colony-forming choanoflagellate *Salpingoeca rosetta*, Dev. Biol. **357**, 73–82 (2011).
[2] S.R. Fairclough, M.J. Dayel and N. King, Multicellular development in a choanoflagellate, Curr. Biol. **20**, R875–R876 (2010).
[3] A. Hallmann, Morphogenesis in the Family Volvocaceae: Different Tactics for Turning an Embryo Right-side Out, Protist **157** 445–461 (2006).
[4] E.E. Ruppert, R.S. Fox, and R.D. Barnes, *Invertebrate Zoology*, 7th ed. (Thomson-Brooks/Cole, Belmont, CA, 2004).
[5] T. C. Day, S. S. Höhn, S. A. Zamani-Dahaj, D. Yanni, A. Burnetti, J. Pentz, A. R. Honerkamp-Smith, H. Wioland, H. R. Sleath, W. C. Ratcliff, *et al.*, Cellular organization in lab-evolved and extant multicellular species obeys a maximum entropy law, eLife **11**, e72707 (2022).
[6] W.C. Ratcliff, R.F. Denison, M. Borrello and M. Travisano, Experimental evolution of multicellularity, Proc. Natl. Acad. Sci. USA **109**, 1595–1600 (2012).
[7] S. Höhn, A. Honerkamp-Smith, P.A. Haas, P. Khuc Trong, and R.E. Goldstein, Dynamics of a *Volvox* Embryo Turning Itself Inside Out, Phys. Rev. Lett. **114**, 178101 (2015).
[8] T. Aste and T. Di Matteo, Emergence of Gamma distributions in granular materials and packing models, Phys. Rev. E **77**, 021309 (2008).
[9] D. J. Daley, D. Vere-Jones, *et al.*, *An Introduction to the Theory of Point Processes: Volume I: Elementary Theory and Methods* (Springer, 2003).
[10] D. Stoyan, W. S. Kendall, S. N. Chiu, and J. Mecke, *Stochastic Geometry and its Applications* (John Wiley & Sons, 2013).
[11] See Supplemental Material at `http://link.aps.org/supplemental/xxx` for analytical and numerical details, and which includes Refs. [12–28].
[12] E. Lukacs, A Characterization of the Gamma Distribution, Ann. Math. Stat. **26**, 319–324 (1955).
[13] P. Findeisen, A simple proof of a classical theorem which characterizes the gamma distribution, Ann. Stat **6**, 1165–1167 (1978).
[14] R. Durrett, *Probability: Theory and Examples*, Vol. 49 (Cambridge University Press, 2019).
[15] R. Pyke, Spacings, J. R. Stat. Soc. B **27**, 395–436 (1965).
[16] D. J. Grabiner, Brownian motion in a Weyl chamber, non-colliding particles, and random matrices, Ann. IHP Prob. Stat. **35**, 177–204 (1999).
[17] D. G. Hobson and W. Werner, Non-Colliding Brownian Motions on the Circle, Bull. Lon. Math. Soc. **28**, 643–650 (1996).
[18] F. J. Dyson, A Brownian-Motion Model for the Eigenvalues of a Random Matrix, J. Math. Phys. **3**, 1191–1198 (1962).
[19] P. Diaconis and M. Shahshahani, On the eigenvalues of random matrices, J. Appl. Prob. **31**, 49–62 (1994).
[20] T. Kemp, Heat Kernel Empirical Laws on $\mathbb{U}(n)$ and $\mathbb{GL}(n)$, J. Theor. Prob. **30**, 397–451 (2017).
[21] J. Møller and S. Zuyev, Gamma-type results and other related properties of Poisson processes, Adv. Appl. Prob. **28**, 662–673 (1996).
[22] J. Møller, *Lectures on random Voronoi tessellations*, Vol. 87 (Springer Science & Business Media, 2012).
[23] E. Gilbert, Random Subdivisions of Space into Crystals, Ann. Math. Stat. **33**, 958–972 (1962).
[24] P. Rathie, On the volume distribution of the typical Poisson–Delaunay cell, J. Appl. Prob. **29**, 740–744 (1992).
[25] H. J. Malik, Exact Distribution of the Product of Independent Generalized Gamma Variables with the Same Shape Parameter, Ann. Math. Stat. **39**, 1751–1752 (1968).
[26] H. Risken, *Fokker-Planck Equation*, (Springer, 1996).
[27] S. Diamond and S. Boyd, CVXPY: A Python-embedded modeling language for convex optimization, J. Mach. Learn. Res. **17**, 2909 (2016).
[28] D. Kraft, A software package for sequential quadratic programming, Forschungsbericht- Deutsche Forschungs- und Versuchsanstalt fur Luft- und Raumfahrt (1988).
[29] L. Cai, N. Friedman, and X. S. Xie, Stochastic protein expression in individual cells at the single molecule level, Nature **440**, 358 (2006).
[30] N. Friedman, L. Cai, and X. S. Xie, Linking stochastic dynamics to population distribution: an analytical framework of gene expression, Phys. Rev. Lett. **97**,

168302 (2006).
[31] A. Hallmann and D. L. Kirk, The developmentally regulated ECM glycoprotein ISG plays an essential role in organizing the ECM and orienting the cells of *Volvox*, J. Cell Sci. **113**, 4605 (2000)
[32] D.J. Skinner, H. Jeckel, A.C. Martin, K. Drescher, and J. Dunkel, Topological packing statistics of living and nonliving matter, Sci. Adv. **9**, eadg126 (2023).
[33] R. Li, C. Ibar, Z. Zhou, S. Moazzeni, A. N. Norris, K. D. Irvine, L. Liu, and H. Lin, E^2 and gamma distributions in polygonal networks, Phys. Rev. Res. **3**, L042001 (2021).
[34] Q. Du, V. Faber, and M. Gunzburger, Centroidal voronoi tessellations: Applications and algorithms, SIAM Rev. **41**, 637 (1999).
[35] C. Ruscher, J. Baschnagel, and J. Farago, The Voronoi liquid, Europhys. Lett. **112**, 66003 (2016).
[36] M. Tanemura, Statistical distributions of poisson voronoi cells in two and three dimensions, FORMA-TOKYO- **18**, 221 (2003).
[37] J.-S. Ferenc and Z. Néda, On the size distribution of Poisson Voronoi cells, Physica A **385**, 518–526 (2007).
[38] D. Weaire, J. Kermode, and J. Wejchert, On the distribution of cell areas in a Voronoi network, Phil. Mag. B **53**, L101–L105 (1986).
[39] Q. Du and D. Wang, The optimal centroidal Voronoi tessellations and the Gersho's conjecture in the three-dimensional space, Comp. Math. Appl. **49**, 1355 (2005).
[40] M.A. Klatt, J. Lovrić, D. Chen, S.C. Kapfer, F.M. Schaller, P.W.A. Schönhöfer, B.S. Gardiner, A.S. Smith, G.E. Schröder-Turk and S. Torquoato, Universal Hidden Order in Amorphous Cellular Geometries, Nat. Comm. **10**, 811 (2019).
[41] T. M. Hain, M. A. Klatt, and G. E. Schröder-Turk, Low-temperature statistical mechanics of the Quantizer problem: Fast quenching and equilibrium cooling of the three-dimensional Voronoi liquid, J. Chem. Phys. **153, 23 (2020)**.
[42] M. Girolami and B. Calderhead, Riemann manifold Langevin and Hamiltonian Monte Carlo methods, J. Roy. Stat. Soc. B **73**, 123 (2011).
[43] S. F. Edwards and R. Oakeshott, Theory of powders, Physica A **157**, 1080 (1989)
[44] L. Atia, *et al.*, Geometric constraints during epithelial jamming, Nat. Phys. **14**, 613–620 (2018).
[45] D. Dereudre, Introduction to the theory of Gibbs point processes, Stochastic Geometry: Modern Research Frontiers, 181 (2019).
[46] D.L. Kirk, *Volvox: Molecular-Genetic Origins of Multicellularity and Cellular Differentiation* (Cambridge Univ. Press, Cambridge, U.K., 1998).
[47] B. von der Heyde, E. L. von der Heyde, A. Srinivasan, S.K. Birwa, S.S.M.H. Höhn, R.E. Goldstein, and A. Hallman, Stochastic geometry and entropy production of a growing extracellular matrix as revealed by localization of the glycoprotein pherophorin-II in *Volvox carteri*, preprint (2024).